Journal of Applied Polymer Science

Dynamic Mechanical and Thermal Properties of the Composites of Thermoplastic Starch and Lanthanum Hydroxide Nanoparticles

Stephen S. Ochigbo,[1*] Adriaan S.Luyt,[1] Julia P. Mofokeng,[1] Željka Antić,[2] Miroslav D. Dramićanin,[2] Vladimir Djoković[2]

[1]Department of Chemistry, University of the Free State, Qwaqwa Campus, Phuthaditjhaba 9866, South Africa

[2]Vinča Institute of Nuclear Sciences, University of Belgrade, 11001 Belgrade, Serbia

*Present address: Department of Chemistry, Federal University of Technology, PMB 65, Minna Niger State, Nigeria

Correspondence to: V. Djoković (E-mail: djokovic@vinca.rs)

ABSTRACT: Nanostructured lanthanum (III)-oxide (La_2O_3) particles were prepared by a polymer complex solution method and further used for the preparation of lanthanum hydroxide ($La(OH)_3$) nanoparticles. The $La(OH)_3$ nanopowder was mixed with glycerol-plasticized maize starch and the effect of the filler on the thermal, mechanical, and viscoelastic properties of the matrix was investigated. It was expected that this nanofiller, which shows an affinity toward OH groups, would strongly affect the physical properties of thermoplastic starch (TPS). The pure TPS and the TPS-$La(OH)_3$ nanocomposite films (with 1, 2, and 3 wt % filler) were conditioned at various relative humidities (RHs) (35, 57, 75, and 99% RH). After conditioning at 99% RH, the pure TPS films exhibited higher affinity toward water than the nanocomposites. Differential scanning calorimetric measurements showed that, due to retrogradation effects, the melting enthalpies of the films increased with increasing RH. Dynamic mechanical analysis revealed that the mechanical properties in the linear range strongly depend on both the humidity conditions and the concentration of the filler. The results also show that $La(OH)_3$ nanoparticles are good reinforcement for TPS films. © 2012 Wiley Periodicals, Inc. J. Appl. Polym. Sci. 000: 000–000, 2012

KEYWORDS: biopolymer; thermoplastic starch; nanocomposites; nanoparticles; dynamic mechanical analysis; differential scanning calorimetric; mechanical properties

Received 12 December 2011; accepted 9 April 2012; published online
DOI: 10.1002/app.37859

INTRODUCTION

Polymers from renewable resources are becoming a subject of increasing interest in current macromolecular science and technology.[1] Dwindling supplies of petroleum and its increasing price together with rising environmental concerns triggered a burst of research activity in this field. To date, various natural polymers have been investigated, but the polysaccharides, especially cellulose, chitosan, and starch, are still the most studied systems.[1,2] Besides potentially useful physical properties of these materials, the investigations are also motivated by their shear abundance and low cost. Starch, a major form of stored carbohydrate in plants, is a renewable biodegradable polymer that appears as a mixture of two main components; amylose, essentially linear O-(1→4)-α-D-glucan, and amylopectin, a highly branched macromolecule consisting of O-(1→4)-α short D-glucopyranose chains linked by O-α-(1→6) glycoside bonds. The physical properties of starches such as gelatinization, solubility, viscosity, and retrogradation strongly depend on the amylose-amylopectin ratio as well as the material conditioning. The amylose content in typical starches is usually in the range from 15 to 30%.

In the last two decades, starch has attracted a lot of attention as a thermoplastic material.[3] The addition of polyol-type plasticizers reduces the glass transition temperature of starch below its decomposition temperature and makes it more flexible.[4] However, despite good mechanical properties, its high hydrophilicity is a major drawback for the successful application of thermoplastic starch (TPS). Blending with some other polymers or introduction of micron-sized and nanosized fillers has been usually used to improve its thermomechanical properties and sensitivity to water.[5] Cellulose fibrils and whiskers are typical fillers used in the preparation of TPS microcomposites and nanocomposites.[6–13] The other approach suggested was the modification of TPS by solution or melt mixing with nanoclays.[14–24] Recently, nanostructured inorganic particles such as SiO_2,[25] ZnO,[26] and $Zr(OH)_4$[27] were successfully used as fillers

for starch. For example, it was found that the tensile strength and water vapor permeability properties of TPS were significantly improved in the presence of zirconium hydroxide nanoparticles stabilized by carboxymethylcellulose (CMC) sodium.[27] In this study, we decided to consider a novel filler and report on the effects of lanthanum hydroxide ($La(OH)_3$) nanoparticles on the physical properties of maize TPS. The $La(OH)_3$ nanoparticles were chosen because they show an affinity for OH groups, and it was expected that they will strongly interact with starch macromolecules, even without the surface modification used, for example, in Refs. 26 and 27. Because of the potential application as ceramics, sorbent, hydrogen storage, and electrode material,[28,29] the preparation of nanostructured $La(OH)_3$ particles, that is, nanospheres, nanorods, and nanowires has received significant attention.[30–35] Here, we applied the polymer complex solution (PCS) method to synthesize the $La(OH)_3$ nanoparticles and investigate their effects on the thermal, mechanical, and viscoelastic properties of the TPS matrix conditioned at various relative humidities (RHs). In addition, we examined the structure and morphology of the obtained nanoparticles.

EXPERIMENTAL

Materials

Lanthanum (III)-oxide powder (99.9%), polyethylene glycol (PEG) with an average molecular weight of 200, and nitric acid were purchased from Alfa Aesar (Karlsruhe, Germany) and used as received. Maize starch (Meritena 100) with an amylose–amylopectin ratio of 25 : 75 is a product of Hungrana, Szabadegyháza, Hungary, whereas glycerol (99%) was supplied by Merck (Pty) Ltd South Africa, Modderfontein, South Africa.

Preparation of La_2O_3 and $La(OH)_3$ Nanopowders

A modified combustion procedure,[36] known as the PCS method, was used for the synthesis of the La_2O_3 nanopowder. As obtained lanthanum (III)-oxide (9 g) was dissolved in hot nitric acid. PEG was added in 1 : 1 mass ratio with respect to La_2O_3 to the obtained solution. After a few hours of stirring at 80°C, a resin-like solid complex was formed. The complex was fired at 800°C in air, which resulted in the formation of nanostructured La_2O_3 particles. To remove the traces of PEG and nitrate ions, as well as to get the pure crystalline phase, the obtained nanopowder was annealed at 800°C for 2 h. Finally, the La_2O_3 nanopowder was left for 24 h in a humid atmosphere (75% RH), which resulted in the formation of $La(OH)_3$ nanoparticles.

Preparation of TPS and TPS-$La(OH)_3$ Nanocomposite Films

The plasticization of the maize starch was performed in two steps. The first step was performed at the Department of Polymer Engineering, Budapest University of Technology and Economics, according to a procedure explained in Ref. 37. The maize starch was dried at 85°C for 72 h at a maximum starch layer thickness of 60 mm. After that, the glycerol (16 wt % relative to dry starch), water (14 wt %), and magnesium stearate (1 wt %) were added and mixed manually. The mixture was fed into a twin screw extruder (90–130–120–90°C from hopper to die). The extrudate was pelletized and stored at 30°C and 65% RH. In the second step, the starch pellets (1.5 g) were dissolved in 20 mL of deionized water by heating at 65°C for 4 h under constant stirring. To that solution, glycerol was added (27.5 wt % relative to the content of pelletized starch) and the heating continued at 70°C using the same stirring speed for another 75 min. TPS films were obtained by casting the obtained solution into plastic Petri dishes and drying at 45°C for 18 h in a still-air glass incubator.

Prior to the preparation of the nanocomposite, an appropriate amount of $La(OH)_3$ nanopowder was dispersed in 15 mL of water and sonicated using a Cole Parmer CP505 ultrasonic processor. The operating frequency was 20 kHz, with 3 s "pulse on" and 1 s "pulse off" resonating cycle. At the end of the sonication, the resulting $La(OH)_3$ water dispersion was immediately added into the glycerol/starch mixture with continuous heating and stirring for another 45 min. The nanocomposite films were obtained by casting the solution onto Petri dishes and drying under the same conditions as in the case of the pure TPS films. The content of the $La(OH)_3$ nanoparticles in the nanocomposite films was chosen to be 1, 2, and 3 wt % relative to the initial amount of starch pellets (1.5 g).

Film Conditioning

TPS is a hygroscopic material and its properties depend on the water content. To investigate the effect of moisture content on the physical properties of the pure TPS and TPS-$La(OH)_3$ nanocomposites, the films were preconditioned for 7 days at room temperature in desiccators with constant humidities of 35, 57, 75, and 98%. The chosen RHs were controlled using saturated solutions of $CaCl_2{\cdot}6H_2O$, $NaBr{\cdot}2H_2O$, NaCl, and $CuSO_4{\cdot}5H_2O$, respectively.

Characterization

Transmission Electron Microscopy. Transmission electron microscopy (TEM) and high resolution TEM (HRTEM) measurements were performed on a Philips (FEI) CM100 transmission electron microscope (Eindhoven, The Netherlands) at 100 kV. A water suspension of the $La(OH)_3$ nanoparticles was deposited onto carbon-coated copper grids of 400 mesh, left to dry in air, and investigated with the microscopes. For comparison, TEM analysis was also performed on the initially prepared La_2O_3 nanopowder, immediately after its preparation.

X-ray Diffractometry. X-ray diffraction analysis of the La_2O_3 and $La(OH)_3$ nanopowders, as well as the TPS-$La(OH)_3$ nanocomposites, was performed on a Philips PW1710 diffractometer with a Cu-K_α source ($\lambda = 1.54$ Å).

Scanning Electron Microscopy. The dispersion of the $La(OH)_3$ filler in the TPS matrix was investigated by scanning electron microscopy (SEM) using a Shimadzu SSX-550 scanning electron microscope (Kyoto, Japan) at an operating voltage of 15 kV. The pure TPS and the nanocomposite films with 2 wt % of $La(OH)_3$ were immersed in liquid nitrogen and then broken. The images of the fracture surfaces were obtained in the back-scattered electrons (BSE) imaging mode. The composition was checked by energy-dispersive X-ray spectroscopy (EDX) using an X-ray microanalysis unit (Shimadzu) attached to the microscope.

Water Absorption. For the water absorption measurements, the pure TPS and the TPS-$La(OH)_3$ nanocomposite films were cut into square samples of 10 × 10 mm^2. The samples were left to

dry in an oven at 100°C for 12 h. Once taken out from the oven, the films were immediately weighed and subsequently conditioned in a desiccator at 98% RH. The samples were removed at specific time intervals (1, 2, 5, 6, 7, 11, and 14 days) and weighed. The water content K was calculated according to the formula:

$$K = \frac{w_2 - w_1}{w_1} 100\%, \quad (1)$$

where w_1 and w_2 are, respectively, the weights of the sample before and after exposure to 98% RH for a specific time. The reported values are the averages of the measurement of at least three identically prepared samples.

Thermal Analysis. Differential scanning calorimetric (DSC) measurements were performed on a PerkinElmer DSC7 differential scanning calorimeter in a nitrogen atmosphere. Samples conditioned at various RHs in sealed DSC pans were heated from 20 to 250°C at a rate of 20°C min^{-1}. From the DSC curves, the melting temperatures (T_m) and melting enthalpies (ΔH_m) were determined as the maxima and areas of the corresponding fusion peaks. The reported values are averages of the measurements of four identically prepared samples.

Thermogravimetric analysis (TGA) of the pure TPS and the TPS-$La(OH)_3$ nanocomposite films conditioned at 57% RH was performed in a PerkinElmer TGA7 thermal analyzer from 30 to 600°C at a rate of 10°C min^{-1}.

Tensile Testing. The tensile properties were investigated using a Hounsfield H5KS tensile tester at room temperature at a crosshead speed of 50 mm min^{-1}. Prior to conditioning (at 35, 57, and 75% RH), the pure TPS and the TPS-$La(OH)_3$ nanocomposite samples were cut into dumbbells with an approximate cross-sectional area of 5 mm × 0.2 mm (which varied slightly depending on the thickness of the film) and a gauge length of 25 mm. At least four specimens were tested for each set of samples, and the mean values were reported. The humidity was closely monitored using a humidity tester, while the laboratory temperature is kept constant using powerful air conditioners. The temperature was monitored with a digital thermometer.

Dynamic Mechanical Analysis. Dynamic mechanical analysis (DMA) curves of the pure TPS and the TPS-$La(OH)_3$ nanocomposites (with 1 and 3 wt % of inorganic content) conditioned at 35, 57, and 75% RHs were recorded in the temperature range from −120 to 150°C on a Perkin Elmer Diamond DMA in stretching mode. Analyses were performed at a frequency of 1 Hz and the heating rate was 2°C min^{-1}. For the DMA measurements, rectangular specimens 20 × 10 × 0.2 mm^3 were used.

RESULTS AND DISCUSSION

Structural and Morphological Analysis

Figure 1 shows the X-ray diffractometry (XRD) patterns of the La_2O_3 and $La(OH)_3$ nanopowders as well as the TPS-$La(OH)_3$ nanocomposite film. The XRD analysis reveals that the initially synthesized powder is monophased, while the peaks correspond to the hexagonal crystal system of La_2O_3 (JCPDS card No. 05-0602). After being held for 24 h in a humid atmosphere, the

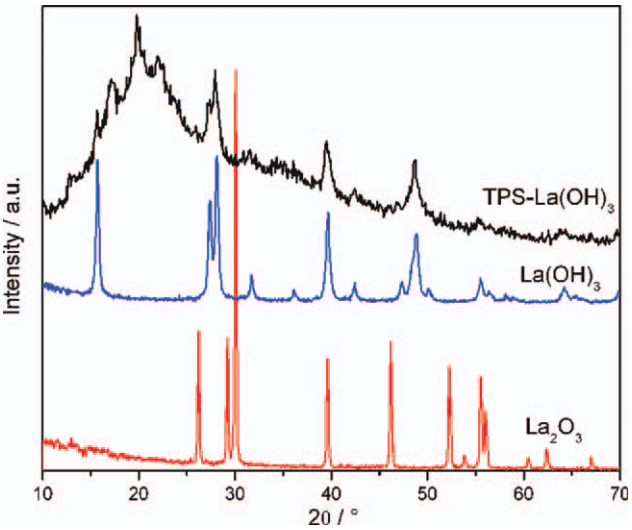

Figure 1. XRD patterns of the TPS-$La(OH)_3$ nanocomposite film, La_2O_3, and $La(OH)_3$ nanopowders. [Color figure can be viewed in the online issue, which is available at wileyonlinelibrary.com.]

La_2O_3 nanopowder spontaneously recrystallizes into $La(OH)_3$.[35] The XRD spectrum of the obtained powder (Figure 1) corresponds to the spectrum of the pure hexagonal phase of lanthanum hydroxide (JCPDS card No. 36-1481). Finally, except for the strong reflections at 15.7, 19.7, and 22° that originate from the starch crystals, the XRD pattern of the nanocomposite film (Figure 1) is basically identical to that of the $La(OH)_3$, suggesting that the nanoparticles maintain their crystal structure after mixing with the polymer.

Figure 2 shows the TEM micrograph of the as-prepared La_2O_3 and $La(OH)_3$ nanoparticles. It can be seen that both the initial La_2O_3 [Figure 2(a)] and the corresponding $La(OH)_3$ [Figure 2(b)] particles have irregular shapes, which is a result of the combustion process. Their sizes are in the range between 50 and 100 nm and they exhibit pronounced agglomeration. In the HRTEM image of the single $La(OH)_3$ particle [Figure 2(b) inset], one can recognize crystal domains with different orientation of crystallographic planes suggesting that the particle is actually polycrystalline.

Preliminary SEM investigations of the gold-coated fractured surfaces of the TPS and the TPS-$La(OH)_3$ nanocomposite films did not provide information about the dispersion of the nanoparticles within the matrix. For this reason, the uncoated fractured surfaces were investigated in BSE mode where the image contrast strongly depends on the atomic number of the elements in the sample. Figure 3 shows the BSE micrograph of the pure TPS and the TPS-$La(OH)_3$ nanocomposite. The BSE micrograph of the pure TPS film [Figure 3(a)] does not provide more information than the image obtained using standard SEM. On the other hand, the BSE micrograph of the nanocomposite sample depicts a large number of nanosized bright formations suggesting that they contain heavier atoms than the surrounding matrix. The nanoparticles are well dispersed in the TPS matrix, but the dispersion is not completely uniform due to clustering. Finally, the EDX spectrum (not shown) revealed

Applied Polymer SCIENCE

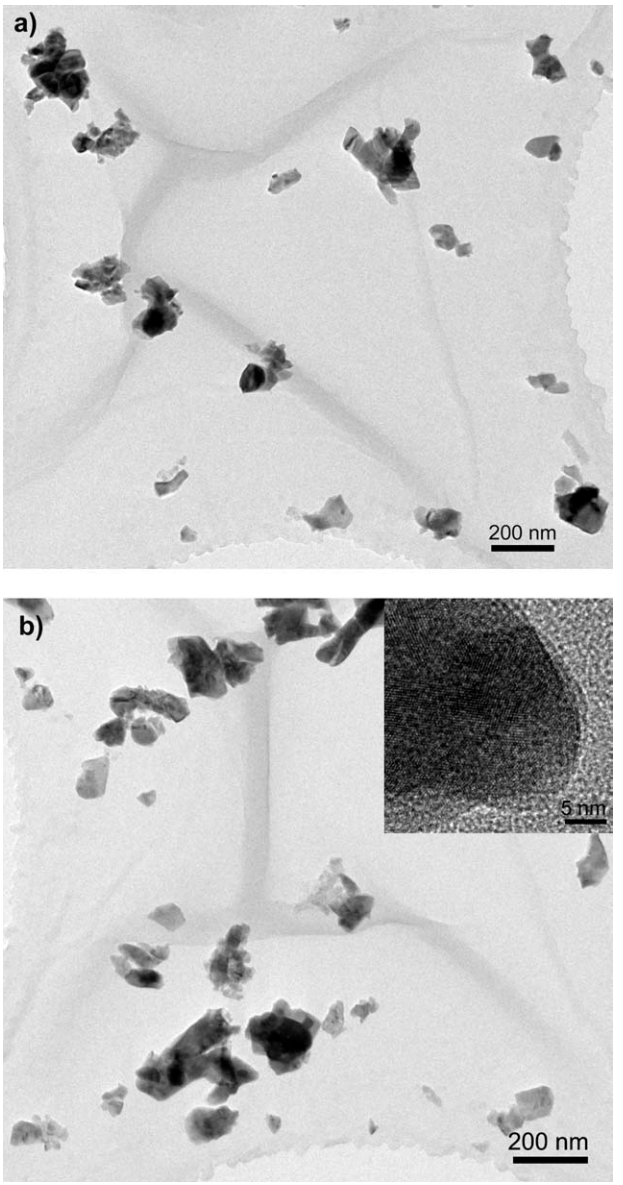

Figure 2. TEM image of the (a) La_2O_3 and (b) $La(OH)_3$ nanoparticles. Inset shows an HRTEM image of a single $La(OH)_3$ particle.

that the observed bright formations contain lanthanum atoms, that is, that they indeed originate from the $La(OH)_3$ nanoparticles.

Water Absorption

In Figure 4, the weight percentage of the water absorbed by the pure TPS and the TPS-$La(OH)_3$ nanocomposites is plotted versus time of exposure to 98% RH. It can be seen that all four materials show similar functional dependence of water absorption on time. There is a rapid water uptake at short times ($t <$ 100 h), while at longer exposure, it reaches a plateau that corresponds to the equilibrium swelling. The mentioned behavior is typical for the pure TPS and its nanocomposites and microcomposites.[7,9,12,20] It should be noticed in Figure 4 that all three nanocomposites show lower values of water uptake than that of the pure TPS along the whole interval of measuring times. This effect might have been the result of the strong interaction of the filler with the matrix chains via OH groups. However, as the observed changes are small (~5–6%) and as the water uptake was measured with respect to the mass of the whole sample and not only with respect to that of the matrix, the former conclusion should be taken with caution. It should also be noticed that the lowest water absorption is observed for the TPS-$La(OH)_3$ nanocomposite with 2 wt % of inorganic content. As the filler loading increases, the effect is reversed, probably due to more pronounced agglomeration of the particles, which affects their interactions with the starch chains.

Thermal Analysis

Differential Scanning Calorimetry. The DSC melting curves of the pure TPS conditioned at various humidities are shown in Figure 5. To enable easier comparison, the curves were baseline corrected (using Pyris software) and shifted along the *y*-axis. The melting enthalpies and melting temperatures that correspond to these curves are given in Table I. It can be seen in Figure 5 that the intensity of the melting peak increases with increasing RH, while at the same time, the position of the peak shifts to lower temperatures. The increase in the melting

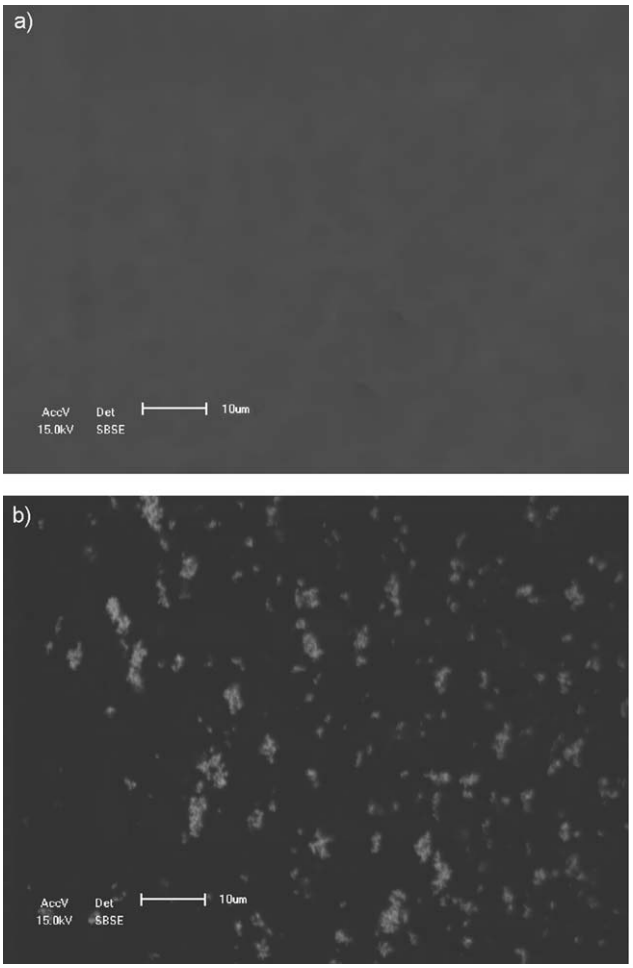

Figure 3. SEM micrograph of the fracture surface of the (a) pure TPS and (b) TPS-$La(OH)_3$ nanocomposite (2 wt % of filler) films obtained in the BSE imaging mode.

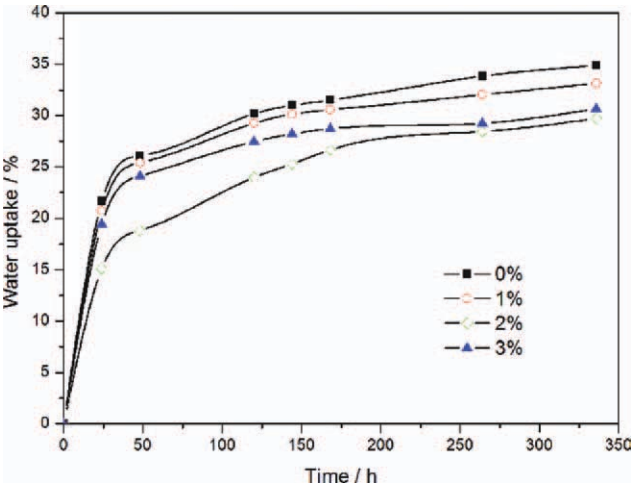

Figure 4. Water uptake versus time for the pure TPS and the TPS-nanocomposite films with 1, 2, and 3 wt % of $La(OH)_3$ nanoparticles. [Color figure can be viewed in the online issue, which is available at wileyonlinelibrary.com.]

enthalpies (i.e., crystallinity) of the samples at higher RH values is a consequence of the well-known retrogradation effect induced by water.[38] It should also be mentioned that evaporation of water during these tests might have affected the obtained results for high humidity samples. The shift of the endothermic peak toward lower temperatures with increasing RH suggests that at lower water contents, the crystals grow into larger domains, while at higher water contents, the crystallization centers are more evenly distributed along the sample, resulting in thinner but more uniformly sized crystals (as the sharpening of melting peak shows). The nanocomposite samples (for one specific $La(OH)_3$ content) showed similar melting behavior with respect to the humidity conditions as the pure TPS. For this reason, we decided to present separately the melting endo-

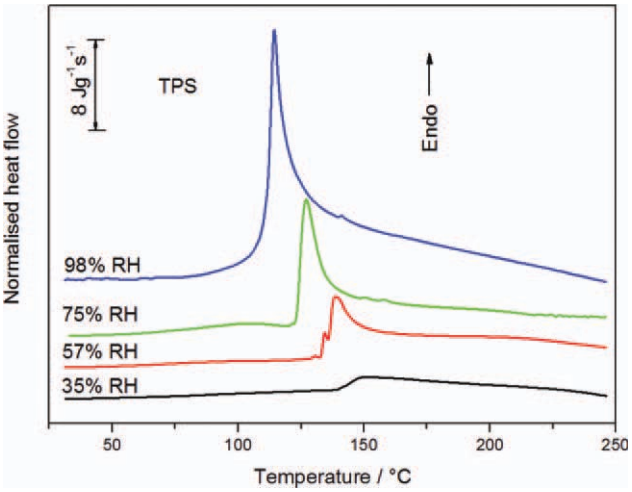

Figure 5. DSC heating curves of the pure TPS films conditioned for 7 days at various RHs (the RH values are given above the corresponding curves). [Color figure can be viewed in the online issue, which is available at wileyonlinelibrary.com.]

Table I. Melting Temperatures (T_m) and Melting Enthalpies (ΔH_m) of TPS-$La(OH)_3$ Nanocomposite Films Conditioned at Different RHs

	35% RH		57% RH		75% RH		99% RH	
$La(OH)_3$/wt %	$T_m \pm \sigma_N$ (°C)	$\Delta H_m \pm \sigma_N$ (J g^{-1})	$T_m \pm \sigma_N$ (°C)	$\Delta H_m \pm \sigma_N$ (J g^{-1})	$T_m \pm \sigma_N$ (°C)	$\Delta H_m \pm \sigma_N$ (J g^{-1})	$T_m \pm \sigma_N$ (°C)	$\Delta H_m \pm \sigma_N$ (J g^{-1})
0	151.5 ± 1.8	38 ± 6	138.6 ± 1.2	95 ± 10	127.7 ± 0.6	227 ± 34	114.2 ± 0.5	332 ± 34
1	155.4 ± 3.2	34 ± 4	139.9 ± 0.8	86 ± 12	131.1 ± 0.8	256 ± 43	119.8 ± 0.9	284 ± 21
2	151.3 ± 1.5	36 ± 5	141.8 ± 0.9	111 ± 16	132.4 ± 0.4	282 ± 15	121.5 ±1.2	292 ± 43
3	156.4 ± 1.4	42 ± 6	146.1 ± 0.9	118 ± 20	137.4 ± 1.5	269 ± 25	123.2 ± 1.0	452 ± 41

Applied Polymer SCIENCE

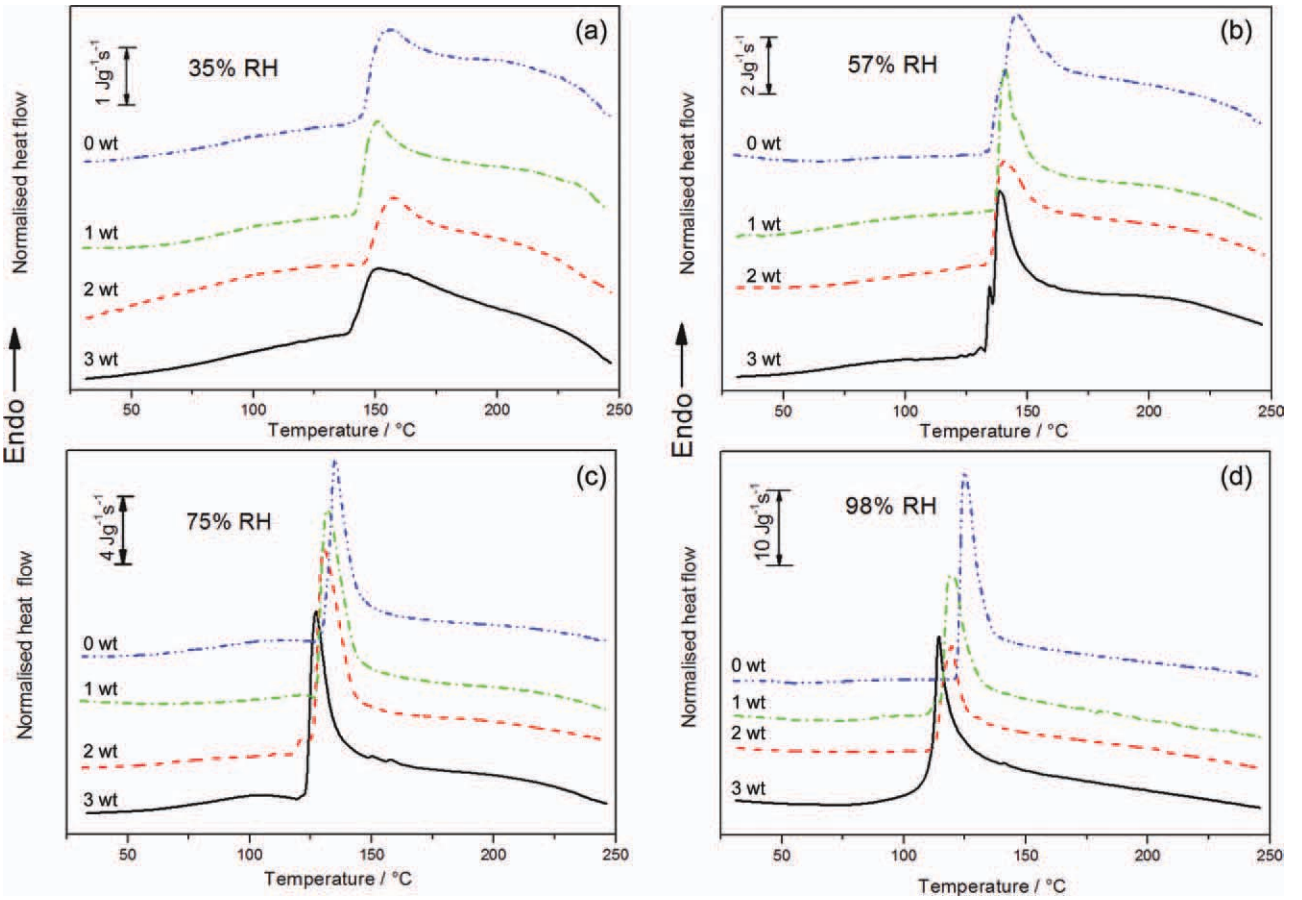

Figure 6. DSC heating curves of the pure TPS and TPS-$La(OH)_3$ nanocomposite films conditioned at (a) 35% RH, (b) 57% RH, (c) 75% RH, and (d) 98% RH. The numbers above the curves indicate the weight content of $La(OH)_3$ in the films. [Color figure can be viewed in the online issue, which is available at wileyonlinelibrary.com.]

therms of the materials at different nanoparticle contents and at fixed RH values. The results are shown in Figure 6. A shift of the melting peak toward higher temperature with increasing nanofiller content can be noticed. The melting peak temperatures (Table I) of the samples conditioned at 35% RH are scattered, but in the case of the other humidities, the peak temperatures clearly increase as the $La(OH)_3$ content increases. The $La(OH)_3$ nanoparticles probably act as nucleating agents for the starch crystallization. This nucleation is probably driven by a pronounced interaction between the OH groups of amylopectin and the nanoparticles.[12] Similar behavior, that is, a shift of the endothermic peak toward higher temperature with increasing filler content, was also observed in the case of TPS-tunicin whiskers nanocomposites.[7] The melting enthalpy results in Table I show that, at a particular RH, the nanoparticles may promote retrogradation. However, this conclusion should be taken with caveat as in some cases the observed changes are within experimental error.

Thermogravimetric Analysis. Figure 7 shows the TGA curves of the pure TPS film and the TPS-$La(OH)_3$ nanocomposites (with 1 and 3 wt % of inorganic content). The two mass loss steps, at around 100 and ~170°C, observed before the onset temperature of TPS degradation, were related to the evaporation of water and glycerol, respectively.[13] It can be also seen in Figure 7 that the process at ~170°C and the main decomposition process at 300°C are affected by the introduction of the filler.

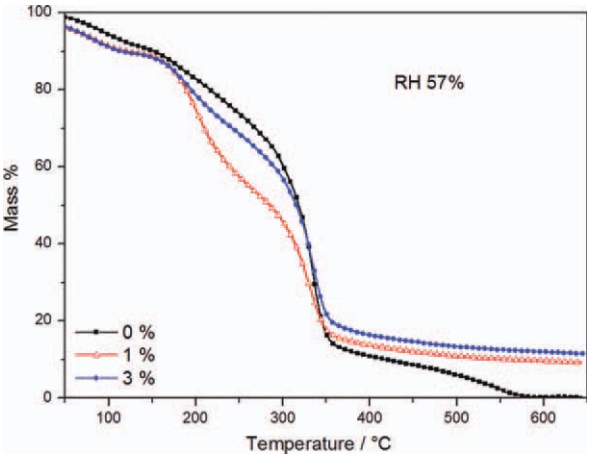

Figure 7. TGA curves of the pure TPS and the TPS-$La(OH)_3$ nanocomposite films with 1 and 3 wt % of filler conditioned at 57% RH (heating rate 10°C min^{-1}). [Color figure can be viewed in the online issue, which is available at wileyonlinelibrary.com.]

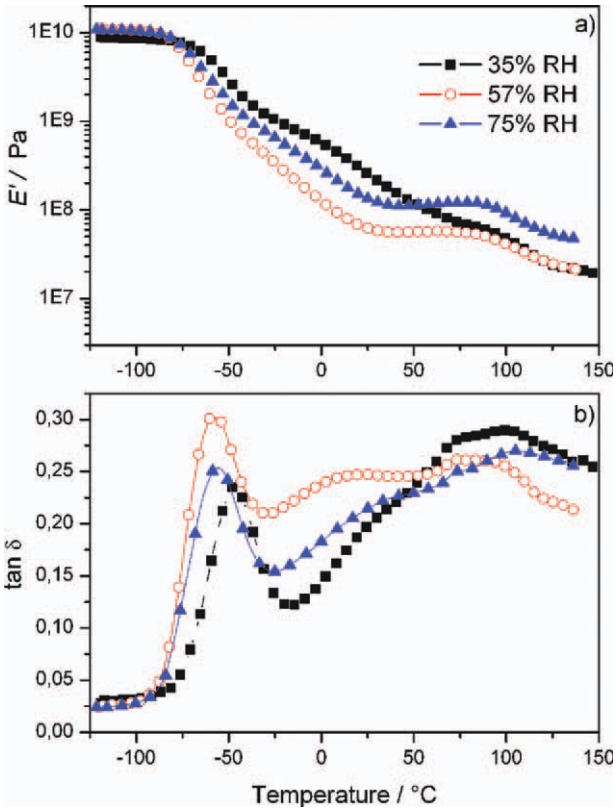

Figure 8. (a) Storage tensile modulus (E') and (b) loss angle tangent (tan δ) versus temperature for the pure TPS films conditioned at 35, 57, and 75% RH. The measurements were performed at 1 Hz. [Color figure can be viewed in the online issue, which is available at wileyonlinelibrary.com.]

The onset of thermal degradation of the nanocomposite is shifted toward lower temperatures compared to that of the pure TPS film. Also, the decomposition of the nanocomposite yields a high ash content at the end of the measurement (~10–15%), whereas the decomposition of the pure starch film leaves no residue. According to a study by Zhang et al.[39] thermal decomposition of starch starts at ~250°C, but a significant mass loss (70–90 wt %) occurs around 300–400°C. In the beginning of the decomposition process, the thermal condensation between hydroxyl groups induces the formation of shorter segments and a loss of water. Because of dehydration, further decomposition takes place via glucose ring scissions and double-bond formation between C-atoms. Formation of aromatic and/or cross-linked structures occurs at about 300°C, while a further increase in temperature (above 400°C) leads to carbonization of the material.[39] As can be seen in Figure 7, the introduction of the $La(OH)_3$ nanoparticles slightly changes the decomposition route of the TPS matrix, and they particularly affect the first decomposition step. There is a higher mass loss at lower temperatures (<300°C), but at the same time, there is a pronounced carbonization of the material at higher temperatures (note that the residue at the end of the decomposition is much higher than the inorganic content in the composite). The reduced thermal stability of the nanocomposite suggests that the processes of thermal condensation are more intense in the presence of the nanoparticles. Similar results were obtained by Liu at al.[27] in the case TPS-$Zr(OH)_4$-CMC nanocomposites. On the other hand, an increase in thermal stability of TPS with the introduction of montmorillonite nanoparticles was also reported.[19,20,24]

DMA (Linear Range)

Figure 8 shows the storage modulus ($E' = \varphi(T)$) and loss tangent (tan $\delta = \varphi(T)$) of the pure TPS films conditioned at various RHs. It can be seen that at low temperatures (−125 to −75°C), there are no significant changes in the storage modulus with variation of the moisture content. In the temperature range from −75 to approximately 50°C, an increase in RH reduces the storage modulus of the films [Figure 8(a)]. On the other hand, at higher temperatures (above 50°C), a faster drop in E' was observed for the sample conditioned at 35% RH. Two main relaxation transitions that correspond to the drop of the modulus can be seen in the tan δ curve at approximately −50 and 100°C [Figure 8(b)], and they are usually termed the "lower" and "upper" transitions, respectively.[40] The existence of these two processes is actually the result of the highly heterogeneous nature of the pure TPS matrix, that is, they originate from the cooperative motions of the chain segments that belong to the glycerol–starch and the pure starch rich domains. The lower transition (labeled here as α_1), which is related to the glass transition of the glycerol–starch mixture, is shifted toward lower temperatures with an increase in the RH. This is in agreement with other results reported in the literature.[8,40] Figure 8(b) also shows that at higher moisture contents, the upper transition (labeled as α_2) appears at higher temperatures, but at the same time, the magnitude of the loss peak decreases. This corresponds to a slower decrease in the storage modulus of the samples conditioned at 57 and 75% RH at temperatures above 75°C, which is probably due to the crystallization of the starch in humid conditions.[8] In the tan δ curves of the three samples [Figure 8(b)], one can see a broad peak shoulder positioned around room temperature. Some authors ascribe this process to moisture loss.[21] On the other hand, the observed shoulder also belongs to the temperature region of the α_2 process.[40] It should be emphasized that the obtained results suggest that even very small losses of moisture occurring during measurements above 0°C can induce drastic changes in the viscoelastic properties. As one of the reviewers of this article pointed out, totally different results may be obtained by only changing the heating rate in the measurements and for this reason, it is extremely difficult to derive definite conclusions about the effects observed in this temperature region.

The storage moduli and loss tangents of the pure TPS and the TPS-$La(OH)_3$ nanocomposite films conditioned at 35% RH are shown in Figure 9. All three materials have similar values of E' in the temperature range investigated here, although, in the case of the nanocomposites, a slight change in the shape of the curves was noticed at temperatures above 50°C [Figure 9(a)]. Concerning the loss curves, Figure 9(b) depicts that increasing in $La(OH)_3$ content induces a shift of the tan δ peaks toward lower temperatures. This means that at low RHs, the plasticization effect of water is more pronounced in the presence of the nanoparticles. The accentuated shoulder positioned at ~25°C

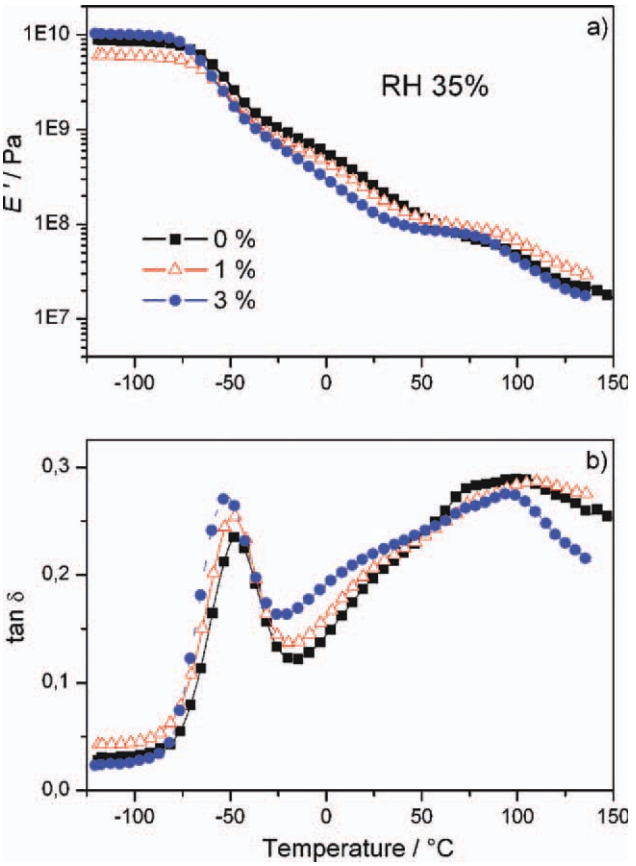

Figure 9. (a) Storage tensile modulus (E') and (b) loss angle tangent (tan δ) versus temperature for the pure TPS and the TPS-$La(OH)_3$ nanocomposite films (with 1 and 3 wt % of filler content) conditioned at 35% RH. The measurements were performed at 1 Hz. [Color figure can be viewed in the online issue, which is available at wileyonlinelibrary.com.]

(attributed above to moisture loss) increases in intensity after nanoparticle addition suggesting that they facilitate release of water during heating.

On the other hand, the pure TPS and nanocomposite films conditioned at 57% RH show opposite behavior. It can be seen in Figure 10(a) that the storage modulus increases as the $La(OH)_3$ content increases. This might have been a consequence of the strong interaction between the nanoparticles and the matrix as well as the higher crystallinity of the nanocomposite samples as observed by DSC (Table I). It is also supported by the increase in the α_1- and α_2-transition temperatures [Figure 10(b)]. The position of the lower transition (α_1) is shifted from −60.3°C for the pure TPS to −53.5°C for the nanocomposite with 3 wt % of $La(OH)_3$. The temperature of the upper transition (α_2) increases from 88.6°C (TPS) to 107.2°C (the nanocomposite with 3 wt % of $La(OH)_3$), which suggests that the nanoparticles penetrate both the glycerol–starch and the pure starch rich domains. Although the SEM micrograph shows that the nanoparticles tend to group in clusters, due to the combined effects of reinforcement and increasing crystallinity, they obviously improve the viscoelastic properties of the TPS matrix. Similar results were reported by Yu et al.[26] for the pure TPS and the TPS-ZnO-CMC nanocomposite films conditioned at 50% RH. Finally, the intensity of the shoulder on the tan δ curves is also reduced meaning that the relaxation related to water loss is also affected by the presence of nanoparticles.

Figure 11 shows the E' and tan δ of the TPS and the nanocomposite films conditioned at 75% RH. It can be seen that the modulus decreases on addition of the $La(OH)_3$ nanoparticles. The observed effect could be the result of more pronounced chain mobility that enables easier diffusion of the plasticizer and its accumulation in the vicinity of the nanoparticle–matrix interfaces.[8] The accumulation of the plasticizer affects the chain-nanoparticle bonding and in turn reduces the reinforcement. This is particularly apparent in the case of the nanocomposite filled with 3 wt % of $La(OH)_3$, where the α_1 transition was shifted toward lower temperatures by almost 10°C. The decrease in the glass transition temperature implies that after conditioning at 75% RH, the weaker interaction between the matrix and the nanoparticles was also accompanied by an increase in the free volume of the chains. Furthermore, in the tan δ spectrum of the nanocomposite with 3 wt % of $La(OH)_3$, an extra peak was observed at about 6°C,

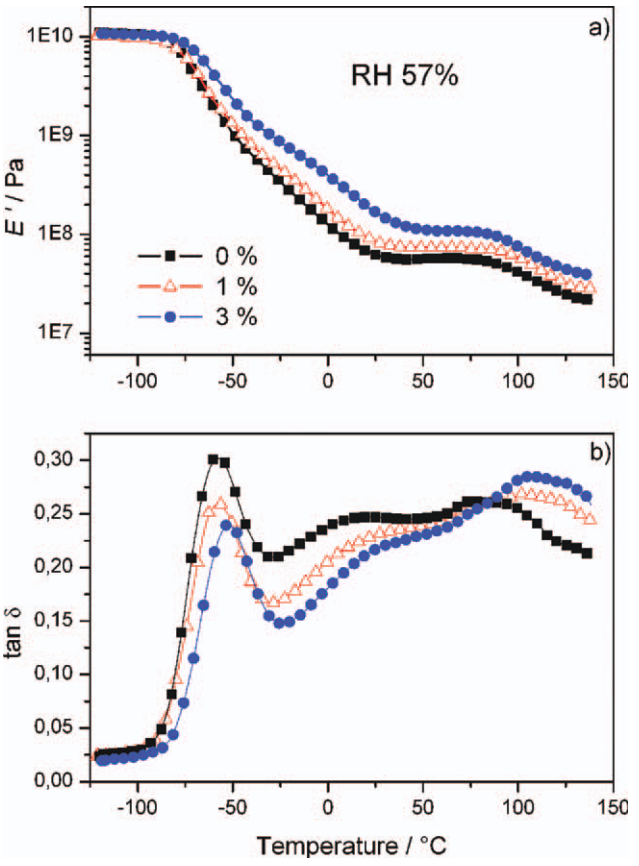

Figure 10. (a) Storage tensile modulus (E') and (b) loss angle tangent (tan δ) versus temperature for the pure TPS and the TPS-$La(OH)_3$ nanocomposite films (with 1 and 3 wt % of filler content) conditioned at 57% RH. The measurements were performed at 1 Hz. [Color figure can be viewed in the online issue, which is available at wileyonlinelibrary.com.]

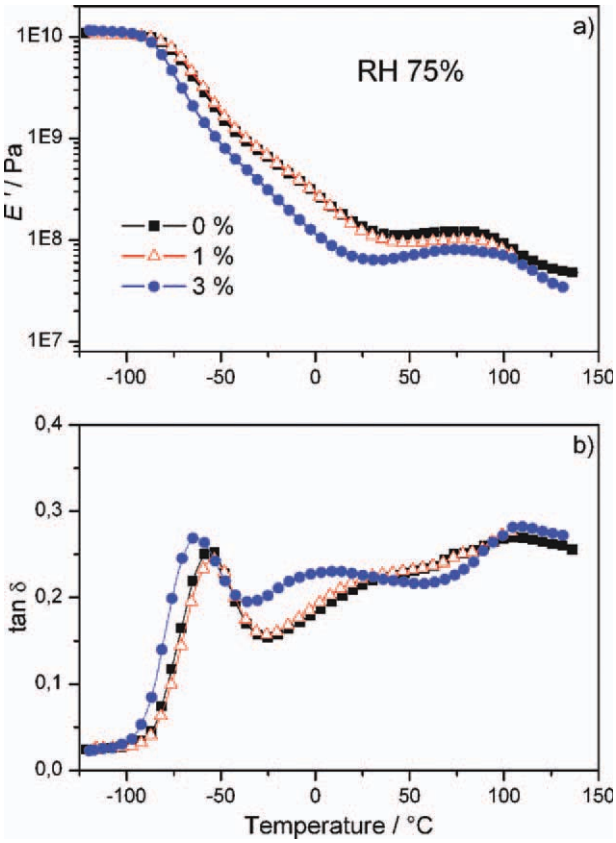

Figure 11. (a) Storage tensile modulus (E') and (b) loss angle tangent (tan δ) versus temperature for the pure TPS and the TPS-La(OH)$_3$ nanocomposite films (with 1 and 3 wt % of filler content) conditioned at 75% RH. The measurements were performed at 1 Hz. [Color figure can be viewed in the online issue, which is available at wileyonlinelibrary.com.]

which suggests some pronounced rearrangements in the matrix during the moister loss. It should be mentioned that Angles and Dufresne[8] also noticed that TPS-tunicin whiskers nanocomposites show lower values of the rubbery modulus with respect to pure TPS after conditioning at higher RHs (58 and 75% RH).

Tensile Testing (Nonlinear Range)

The nonlinear mechanical behavior of pure TPS and TPS-La(OH)$_3$ nanocomposite films conditioned at 35, 57, and 75% RH was studied at room temperature. The obtained tensile parameters, for example, Young's modulus, tensile strength, and elongation at break are plotted versus nanofiller content in Figure 12. The values inserted for the pure TPS matrix correspond to zero filler content. As the conditioned starch films contain both amorphous and crystalline domains, the reported moduli in average reflect the contributions of each phase.[8] Besides the La(OH)$_3$ particles, the crystalline domains also act as filler in the amorphous matrix affecting the mechanical properties. Because of the plasticization effects of water, Young's modulus decreases with increasing the moisture content in all the studied samples [Figure 12(a)]. Depending on the humidity conditions and the La(OH)$_3$ content, the moduli range between 10 and 80 MPa. In the case of the pure TPS samples, the obtained modulus values are in agreement with the results of Angles and Dufresne[8] but lower than those reported in the study of Kumar and Singh.[12] Figure 12(a) also shows that the modulus of the samples, conditioned at 35 and 57% RH, increases with more than 50% with the introduction of 1 wt % La(OH)$_3$, but slightly decreases with further increase in the inorganic content. The latter effect might be the result of the more pronounced clustering of the nanoparticles at higher filler loadings. On the other hand, the modulus of the samples conditioned at the highest RH (75% RH) is virtually independent from the concentration of the filler, which is also in agreement with literature data.[8] It is worth mentioning that the presence of the shoulder at ~25°C observed in the DMA curves (Figures 8–11) suggests that the pure TPS and the TPS-nanocomposites are very sensitive to temperature fluctuation in the temperature region in the vicinity of room temperature. The fact that much lower stresses were used in DMA measurements (which do not significantly affect the structure of the samples) and that in this temperature region moisture release occurs during DMA heating, makes difficult the comparison of the Young's moduli obtained in DMA (Figure 8) and tensile

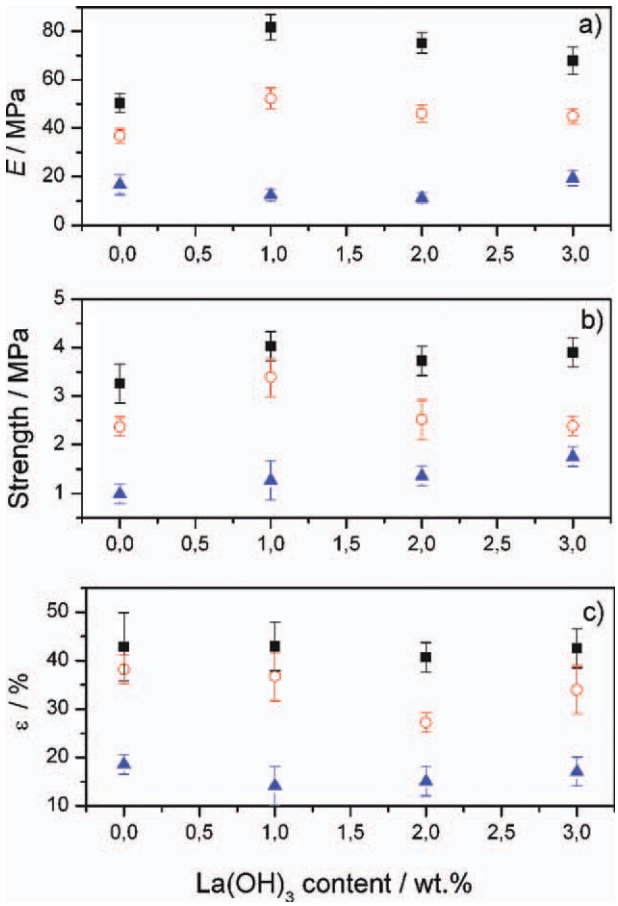

Figure 12. (a) Young's modulus, (b) tensile strength, and (c) strain at break of the studied films versus La(OH)$_3$ content. The films were conditioned at 35% RH (■), 57% RH (○), and 75% RH (▲). [Color figure can be viewed in the online issue, which is available at wileyonlinelibrary.com.]

testing (Figure 12) measurements. For this reason, the experimental conditions (RH and temperature) during the tensile measurements were strictly controlled.

The ultimate properties (tensile strength and strain at break) of the unfilled TPS and the TPS-$La(OH)_3$ nanocomposite films are shown in Figure 12(b, c). During the tensile test, the wet materials behaved slightly different from the dry ones. In the samples conditioned in very humid atmospheres (57 and 75% RH), tearing before break was noticed. For these samples, instead of the true stress at break, the highest stress observed before tearing is reported. The values of the tensile strength ranged from 1 to 4 MPa. Again, due to the restricted mobility of the matrix chains imposed by the filler, an increase in strength of about 30% was noticed for the samples with 1 wt % $La(OH)_3$ at lower humidities (35 and 57% RH). At higher filler contents (2 and 3 wt %), the tensile strength either stays virtually unchanged (35% RH) or slightly decreases (57% RH). This behavior is different than that reported for TPS-ZnO-CMC[26] and TPS-$Zr(OH)_4$-CMC[27] nanocomposites, where the tensile strength of the films conditioned at 50% RH increased steadily with increase in the concentration of the filler. On the other hand, the results presented in Figure 12(b) are in agreement with those obtained for TPS-tunicin whiskers nanocomposites[8] at low filler contents. Figure 12(b) also shows that the samples conditioned at 75% RH exhibit an almost linear dependence of strength on the $La(OH)_3$ content. Concerning strain at break, it decreases with increasing in RH but it does not change significantly with an increase in the concentration of the filler [Figure 12(c)].

CONCLUSIONS

In conclusion, the introduction of a $La(OH)_3$ nanofiller into a TPS matrix improves its physical properties. However, the reported results depended on both the concentration of the filler and the moisture content. The influence of the filler on the mechanical and viscoelastic properties was more pronounced in the nanocomposite films conditioned at lower RHs (35 and 57% RH). At these RHs, the nanocomposites with 1 wt % of $La(OH)_3$ particles showed much higher values of elastic modulus (>50%) and tensile strength (>30%) than those of the pure TPS films, suggesting that 1 wt % is the optimal filler content for TPS. Also, in the case of the films conditioned at 57% RH, the nanoparticles improve the storage modulus and induce a shift of the two main transitions in the tan δ (DMA) spectra toward higher temperatures. DSC measurements showed that the crystallinity of the films depended mostly on the humidity conditions and less on the concentration of the filler. On the other hand, the position of the endothermic peak was shifted toward higher temperatures with an increase in inorganic content.

REFERENCES

1. Gandini, A. Macromolecules **2008,** *41*, 9491.
2. Kumar, M. N. *V. R. React. Funct. Polym.* **2000,** *46*, 1.
3. Carvalho, A. J. F. In Monomers, Polymers and Composites from Renewable Resources; Belgacem, M. N.; Gandini A., Eds.; Elsevier: Amsterdam, **2008;** Chapter 15, pp 321–342.
4. Galdeano, M. C.; Suzana Mali, S.; Grossmann, M. V. E.; Yamashita, F.; García, M. A. *Mater. Sci. Eng. C* **2009,** *2*, 532.
5. Yu, L.; Deana, K.; Lib, L. *Prog. Polym. Sci.* **2006,** *31*, 576.
6. Dufresne, A.; Vignon, M. R. *Macromolecules* **1998,** *31*, 2693.
7. Angles, M. N.; Dufresne, A. *Macromolecules* **2000,** *33*, 8344.
8. Angles, M. N.; Dufresne, A. *Macromolecules* **2001,** *33*, 2921.
9. Mathew, A. P.; Dufresne, A. *Biomacromolecules* **2002,** *3*, 609.
10. Dufresne, A.; Dupeyre, D.; Vignon, M. R. *J. Appl. Polym. Sci.* **2000,** *76*, 2080.
11. Curvelo, A.; de Carvalho, A.; Agnelli, J. *Carbohydr. Polym.* **2001,** *45*, 183.
12. Kumar, A. P.; Singh, R. P. *Bioresour. Technol.* **2008,** *99*, 8803.
13. Martins, I. M. G.; Magina, S. P.; Oliveira, L.; Freire, C. S. R.; Silvestre, A. J. D.; Neto, C. P.; Gandini A. *Compos. Sci. Technol.* **2009,** *69*, 2163.
14. Almasi, H.; Ghanbarzadeh, B.; Entezami, A. A. *Int. J. Biol. Macromol.* **2010,** *46*, 1.
15. Majdzadeh-Ardakani, K.; Navarchian, A. H.; Sadeghi, F. *Carbohydr. Polym.* **2010,** *79*, 547.
16. Wang, N.; Zhang, X. X.; Han, N.; Bai, S. H. *Carbohydr. Polym.* **2009,** *76*, 68.
17. Dai, H. G.; Chang, P. R.; Geng, F. Y.; Yu, J. G.; Ma, X. F. *J. Polym. Environ.* **2009,** *17*, 225.
18. Tang, X. Z.; Alavi, S.; Herald, T. J. *Carbohydr. Polym.* **2008,** *74*, 552.
19. Huang, M. F.; Yu, J. G.; Ma, X. F.; Jin, P. *Polymer* **2005,** *46*, 3157.
20. Huang, M. F.; Yu, J.; Ma, X. F. *Polymer* **2004,** *45*, 7017.
21. Wilhelm, H. M.; Sierakowski, M. R.; Souza, G. P.; Wypych, F. *Carbohydr. Polym.* **2003,** *52*, 101.
22. McGlashan, S. A.; Halley, P. J. *Polym. Int.* **2003,** *52*, 1767.
23. Park, H. M.; Li, X.; Jin, C. Z.; Park, C. Y.; Cho, W. J.; Ha, C. S. *Macromol. Mater. Eng.* **2002,** *287*, 553.
24. Park, H. M.; Lee, W. K.; Park, C. Y.; Cho, W. J.; Ha, C. S. *J. Mater. Sci.* **2003,** *38*, 909.
25. Wu, M.; Wang, Y.; Wang, M.; Ge, M. *Fibres Text. East. Eur.* **2008,** *16*, 96.
26. Yu, J.; Yang, J.; Liu, B.; Ma, X. *Bioresour. Technol.* **2009,** *100*, 2832.
27. Liu, D.; Chang, P. R.; Deng, S.; Wang, C.; Zhang, B.; Tian, Y.; Huang, S.; Yao, J.; Ma, X. *Carbohydr. Polym.* **2011,** *86*, 1699.
28. Zhu, J. L.; Zhou, Y. H.; Yang, H. J. *J. Power Sources* **1997,** *69*, 169.
29. Niu, F.; Cao, A. M.; Song, W. G.; Wan, L. J. *J. Phys. Chem. C* **2008,** *112*, 17988.
30. Jia, G.; Huang, Y.; Song, Y.; Yang, M.; Zhang, L.; You, H. *Eur. J. Inorg. Chem.* **2009,** *25*, 3721.

31. Salavati-Niasari, M.; Hosseinzadeh, G.; Davar, F. J. *Alloys Compd.* **2011,** *509*, 4098.
32. Tang, B.; Ge, J.; Zhuo, L. *Nanotechnology* **2004,** *15*, 1749.
33. Tang, B.; Ge, J.; Wu, C.; Zhuo, L.; Niu, J.; Chen, Z.; Shi, Z.; Dong, Y. *Nanotechnology* **2004,** *15*, 1273.
34. Wang, X.; Li, Y. *Angew. Chem. Int. Ed.* **2002,** *41*, 4790.
35. Fleming, P.; Farrell, R. A.; Holmes, J. D.; Morris, M. A. *J. Am. Ceram. Soc.* **2010,** *93*, 1187.
36. Andrić, Ž.; Dramićanin, M. D.; Mitrić, M.; Jokanović, V.; Bessière, A.; Viana, B. *Opt. Mater.* **2008,** *30*, 1023.
37. Tábi, T.; Kovács, J. G. *Express Polym. Lett.* **2007,** *1*, 804.
38. De Meuter, P.; Hemelrijck, J.; Rahier, H.; Van Mele, B. J. *Polym. Sci. Pol. Phys.* **1999,** *37*, 2881.
39. Zhang, X. Q.; Golding, J.; Burgar, I. *Polymer* **2002,** *43*, 5791.
40. Forssella, P. M.; Mikkilti, J. M.; Moates, G. K.; Parker, R. *Carbohydr. Polym.* **1997,** *34*, 275.